

Analytical Approximations to the Low-Order Statistics of Dark Matter Distribution

H.J. Mo, Y.P. Jing, G. Börner

Max-Planck-Institut für Astrophysik, Karl-Schwarzschild-Strasse 1, 85748 Garching,
Germany

ABSTRACT

We show that in a hierarchical clustering model the low-order statistics of the density and the peculiar velocity fields can all be modelled semianalytically for a given cosmology and an initial density perturbation power spectrum $P(k)$. We present such models for the two-point correlation function $\xi(r)$, the amplitude Q of the three-point correlation function, the mean pairwise peculiar velocity $\langle v_{12}(r) \rangle$, the pairwise peculiar velocity dispersion $\langle v_{12}^2(r) \rangle$, and the one-point peculiar velocity dispersion $\langle v_1^2 \rangle$. We test our models against results derived from N-body simulations. These models allow us to understand in detail how these statistics depend on $P(k)$ and cosmological parameters. They can also help to interpret, and maybe correct for, sampling effects when these statistics are estimated from observations. The dependence of the small-scale pairwise peculiar velocity dispersion on rich clusters in the sample, for instance, can be studied quantitatively. There are also significant implications for the reconstruction of the cosmic density field from measurements in redshift space.

Subject headings: galaxies: clustering - galaxies: distances and redshifts - large-scale structure of Universe - cosmology: theory - dark matter

1. INTRODUCTION

The large scale structure of the Universe is believed to have developed from small perturbations (usually assumed to be Gaussian) of the matter density field by gravitational instabilities. Under these assumptions the clustering pattern and velocity field observed today are determined by the initial conditions via the perturbation power spectrum $[P(k)]$ and the cosmological parameters such as Ω_0 , the cosmic density parameter. It is therefore possible to derive constraints on model parameters from the observed density and velocity distributions of galaxies.

There are two fundamental problems that must be addressed here: First, since it is unlikely that galaxies are completely unbiased testing particles of the matter density field, we need to understand any such bias in order to make meaningful comparisons between models and the observations of the galaxy distribution. Second, even if the observed galaxy distribution traces the matter distribution, we still need to understand how the observed distribution is related to the parameters that describe a cosmogonical model. The latter is by no means trivial, because the clustering pattern and velocity field observed today are nonlinear. N-body simulations are usually invoked to find a solution to this problem. However, as discussed comprehensively by Peebles (1980), a complete statistical description of the clustering process is also provided by the whole BBGKY hierarchy for the distribution function of mass particles. Indeed, adding some assumptions, one can solve the low order moments of the distribution function directly from the BBGKY equations. Although an incomplete description, such solutions are extremely useful for us to gain physical insights into the clustering process. These low order moments are also the most important ones, not only because they describe the most fundamental part of the clustering process but also because in practice they are the ones that can be measured from observations.

In this paper, we show that semianalytical models can be constructed for all low order moments of the distribution function. These models allow such moments to be calculated directly from the initial density perturbation power spectrum for a given cosmological model, and thus provide us with a clear picture of how these moments are related to various model parameters. We present our models and test them against results from N-body simulations in Section 2. In Section 3 we demonstrate how our models can be used to help us to understand better some sampling effects when these moments are to be estimated from observations. Finally, in Section 4 we discuss the implications of our models to the reconstruction of real-space quantities from redshift distortions, and to the construction of some new statistics that can discriminate current models of structure formation.

2. MODELS AND TEST BY N-BODY SIMULATIONS

In this paper we will consider cosmogonies in which the Universe is dominated by cold dark matter (CDM). The cosmology is described by the cosmological matter density (Ω_0), the cosmological constant (λ_0) and the Hubble constant ($H_0 = 100h \text{ km s}^{-1} \text{ Mpc}^{-1}$). When $\lambda_0 \neq 0$, we assume the universe to be flat so that $\Omega_0 + \lambda_0 = 1$.

The initial power spectrum is [Bardeen et al. (1986)]:

$$P(k) \propto kT^2(k), \tag{1a}$$

with

$$T(k) = \frac{\ln(1 + 2.34q)}{2.34q} \left[1 + 3.89q + (16.1q)^2 + (5.46q)^3 + (6.71q)^4 \right]^{-1/4} \quad (1b)$$

and

$$q \equiv \frac{k}{\Gamma h \text{ Mpc}^{-1}}. \quad (1c)$$

Following Efstathiou et al. (1992), we have introduced a shape parameter, $\Gamma \equiv \Omega_0 h$, for the power spectrum. (Note that the Γ defined here is not exactly the same as that of Efstathiou et al.). When Γ is treated as a free parameter, equation (1) can also be used to describe the power spectra in other structure formation models, such as the mixed dark matter (MDM) models (see e.g. Ma 1996). The rms mass fluctuation in top-hat windows with radius R , $\sigma(R)$, is defined by

$$\sigma^2(R) = \int_0^\infty \frac{dk}{k} \Delta^2(k) W^2(kR), \quad (2a)$$

where

$$W(x) = \frac{3(\sin x - x \cos x)}{x^3} \quad (2b)$$

is the Fourier transform of the top-hat window function, and

$$\Delta^2(k) = \frac{1}{2\pi^2} k^3 P(k). \quad (3)$$

For convenience, we will refer to $\Delta^2(k)$ as the power variance. We normalize $P(k)$ by specifying $\sigma_8 \equiv \sigma(8 h^{-1} \text{Mpc})$.

2.1. N-Body Simulations

Before presenting our analytic approximations, we first give a brief summary of the N-body simulations to be used to test the models.

We will use results derived from various P³M N-body simulations (see Jing et al. 1995 for details on these simulations). Each simulation can be characterized by four model parameters ($\Omega_0, \lambda_0, \Gamma, \sigma_8$), as discussed above, and three simulation parameters: the box size L (in $h^{-1} \text{Mpc}$), the number of simulation particles N_p and the effective force resolution ϵ (in $h^{-1} \text{Mpc}$). The model and simulation parameters for all simulations are listed in Table 1. For each simulation we give it a name which is listed in the first column of the table and will be used throughout the paper to refer to the simulation.

2.2. The Two-Point Correlation Function

The evolved two-point correlation function $\xi(r)$ is related to the *evolved* power variance $\Delta_E^2(k)$ by

$$\xi(r) = \int_0^\infty \frac{dk}{k} \Delta_E^2(k) \frac{\sin kr}{kr}. \quad (4)$$

Thus, in order to get $\xi(r)$ we need an expression for $\Delta_E(k)$. Following the original argument of Hamilton et al. (1991), Peacock & Dodds (1994), Jain, Mo & White (1995), Padmanabhan et al. (1996) and Peacock & Dodds (1996, hereafter PD) have obtained fitting formulae which relate Δ_E to the initial density spectrum for a given cosmological model. The latest version of such a fitting formula is given in PD. PD have checked their fitting formula for $\Delta_E(k)$ by a set of N-body simulations. Here we use that formula and provide new tests for its predictions for $\xi(r)$ using results from (independent) N-body simulations.

The evolved power variance Δ_E is assumed to be a function of its linear counterpart Δ :

$$\Delta_E^2(k_E) = f[\Delta^2(k_L)], \quad (5)$$

where $k_L \equiv [1 + \Delta_E^2(k_E)]^{-1/3} k_E$. The functional form of f is approximated by (see PD for details)

$$f(x) = x \left[\frac{1 + \mathcal{R}(x)}{1 + \mathcal{Q}(x)} \right]^{1/\beta}, \quad (6)$$

where

$$\mathcal{R}(x) = B\beta x + (Ax)^{\alpha\beta}, \quad (7a)$$

$$\mathcal{Q}(x) = A^{\alpha\beta} [g(a)]^{3\beta} V^{-\beta} x^{(\alpha-1/2)\beta}, \quad (7b)$$

with

$$A = 0.482[1 + n(k_L)/3]^{-0.947}, \quad (8a)$$

$$B = 0.226[1 + n(k_L)/3]^{-1.778}, \quad (8b)$$

$$V = 11.55[1 + n(k_L)/3]^{-0.423}, \quad (8c)$$

$$\alpha = 3.310[1 + n(k_L)/3]^{-0.244}, \quad (8d)$$

$$\beta = 0.862[1 + n(k_L)/3]^{-0.287}, \quad (8e)$$

$$n(k_L) \equiv \frac{d \ln P}{d \ln k}(k = k_L/2). \quad (8f)$$

The function $g(a)$ in equation (7b) is the linear growth factor at the cosmic time corresponding to the expansion factor a , and for given Ω_0 and λ_0 , it is accurately described by (see Carroll, Press & Turner 1992):

$$g(a) = \frac{5}{2}\Omega \left[\Omega^{4/7} - \lambda + (1 + \Omega/2)(1 + \lambda/70) \right]^{-1}, \quad (9a)$$

where

$$\Omega \equiv \Omega(a) = \frac{\Omega_0}{a + \Omega_0(1 - a) + \lambda_0(a^3 - a)}, \quad (9b)$$

$$\lambda \equiv \lambda(a) = \frac{a^3 \lambda_0}{a + \Omega_0(1 - a) + \lambda_0(a^3 - a)}. \quad (9c)$$

For later use we also define

$$D(a) \equiv ag(a). \quad (9d)$$

It is clear that Δ_E at any wavenumber is determined by Δ for a given cosmology, and we can just use equation (4) to obtain $\xi(r)$. In practice we start with the initial power variance $\Delta(k)$ to obtain a table of $[k_E, \Delta_E(k_E)]$. An interpolation is then used to carry out the integration in equation (4).

The solid curves in Figure 1 show the model predictions for $\xi(r)$ in the SCDM models with $\sigma_8 = 1.24$ and 0.62 , and in the FLAT and OPEN models with $\sigma_8 = 1$. These predictions are compared to the results of N-body simulations shown by the symbols. For SCDM model with $\sigma_8 = 0.62$, two different simulation box sizes are used to show the effects of both finite box size and finite simulation resolution on small scales. It is clear that the fitting formula works well for all cases. We have also obtained results for other models (i.e. FLAT models with $\Omega_0 = 0.3$ and 0.1 , OPEN models with $\Omega_0 = 0.3$ and 0.1 , all having $\sigma_8 = 1$) and found a similar good agreement between model predictions and simulation results.

2.3. The Mean Pairwise Peculiar Velocities

From the pair conservation equation (Peebles 1980, §71), the ensemble (pair weighted) average of the pairwise peculiar velocity $\langle v_{12}(r) \rangle \equiv \langle [\mathbf{v}(\mathbf{x}) - \mathbf{v}(\mathbf{x} + \mathbf{r})] \cdot \hat{\mathbf{r}} \rangle$ can be written as

$$\frac{\langle v_{12}(r) \rangle}{Hr} = -\frac{1}{3} \frac{1}{[1 + \xi(y, a)]} \frac{\partial \bar{\xi}(y, a)}{\partial \ln a}, \quad (10a)$$

where r is the proper, and y the comoving, separation between the pairs;

$$H = H_0 \left[\lambda_0(1 - a^{-2}) + \Omega_0(a^{-3} - a^{-2}) + a^{-2} \right]^{1/2} \quad (10b)$$

is the value of Hubble’s constant for an expansion factor a ;

$$\bar{\xi}(y, a) \equiv \frac{3}{y^3} \int_0^y y^2 dy \xi(y, a) = \int_0^\infty \frac{dk}{k} \Delta_E^2(k, a) W(ky). \quad (10c)$$

Thus, in order to obtain $\langle v_{12}(r) \rangle$, we need to work out $\partial \Delta_E(k, a) / \partial a$. Using the formulae presented in Subsection 2.2, it is straightforward to calculate the derivative $\partial \Delta_E / \partial a$. In Appendix A, an explicit expression is given for this derivative.

Figure 2 shows the comparison between the model prediction of $\langle v_{12}(r) \rangle$ and the simulation result. The agreement between the two is remarkably good for all cases except for B-SCDM0.62 where simulation result is significantly smaller than model prediction on $r \lesssim h^{-1} \text{Mpc}$ (the reason for this will be discussed below). This agreement shows again that the model of $\xi(r)$ presented in §2.2 is also valid for describing the time evolution of $\xi(r)$. Jain (1996) used the time evolution of the two-point correlation function derived directly from N-body simulations to solve for $\langle v_{12}(r) \rangle$ from the pair-conservation equation. The validity of our analytical model shows that $\langle v_{12}(r) \rangle$ can easily be calculated from the initial density spectrum via a single integration. The discrepancy between model prediction and simulation result for the case of B-SCDM0.62 is apparently due to the fact that this simulation is an intermediate output of SCDM1.24 and has evolved only by a factor of 4.5 in the linear density growth factor since the initial simulation time. The numerical artifact of the initial density field generated by the Zel’dovich approximation should exist to some extent when the system is not sufficiently evolved. However, this artifact is expected to become smaller as the simulation evolves, as demonstrated by Baugh et al. (1995). It is therefore gratifying to see that the agreement between model prediction and simulation result is indeed better for SCDM1.24 than for B-SCDM0.62.

2.4. Cosmic Energy Equation

The (density weighted) mean square peculiar velocity of mass particles $\langle v_1^2 \rangle$ is related to the two-point correlation function by the cosmic energy equation:

$$\frac{d}{da} a^2 \langle v_1^2 \rangle = 4\pi G \bar{\rho} a^3 \frac{\partial I_2(a)}{\partial \ln a}, \quad (11)$$

where $\bar{\rho}$ is the mean density of the universe, and

$$I_2(a) \equiv \int_0^\infty y dy \xi(y, a) = \int_0^\infty \frac{dk}{k} \frac{\Delta_E^2(k, a)}{k^2}. \quad (12)$$

Integrating equation (11) once, we have

$$\langle v_1^2 \rangle = \frac{3}{2} \Omega(a) H^2(a) a^2 I_2(a) \left[1 - \frac{1}{a I_2(a)} \int_0^a I_2(a) da \right]. \quad (13)$$

In the linear case, $I_2(a) \propto D^2(a)$ and

$$\langle v_1^2 \rangle = \frac{3}{2} \Omega(a) H^2(a) a^2 I_2(a) \left[1 - \frac{1}{a D^2(a)} \int_0^a D^2(a) da \right]. \quad (14)$$

We have found that equation (14) is a good approximation (to an error of $< 10\%$) to equation (13) for all realistic cases. Thus, for a given cosmogonic model, we can easily obtain $\langle v_1^2 \rangle$.

In Table 2 we compare the values of $\langle v_1^2 \rangle$ calculated from equation (14) to those obtained from N-body simulations. As one can see from equation (12), the contribution to $\langle v_1^2 \rangle$ from the power at small wavenumbers is not negligible, and the values of $\langle v_1^2 \rangle$ derived from the simulations may be sensitive to the loss of power at $k < 2\pi/L$. To see such an effect, we exclude from our analytic calculations all modes with $k < 2\pi/L$. This is done by setting the lower limit of the integration on the right hand side of equation (12) to be $2\pi/L$. The results are given in the left column under the column head ‘ $\langle v_1^2 \rangle^{1/2}$ (model)’. For comparison, the values in brackets are obtained by assuming $L = \infty$. As one can see, the effect of finite box size is indeed significant when the simulation box size is small. This effect is more important for the FLAT and OPEN models than for the SCDM model, because they have more power on large scales. Table 2 shows that the agreement between our model predictions and simulation results is reasonably good.

2.5. Pairwise Peculiar Velocity Dispersion

The relative velocity dispersion of particle pairs of separation r is defined as $\langle [\mathbf{v}(\mathbf{x}) - \mathbf{v}(\mathbf{x} + \mathbf{r})]^2 \rangle^{1/2}$. In Fig.3 we show (by symbols) the dispersion of the pairwise peculiar velocities projected along the separations of particle pairs ($\langle v_{12}^2(r) \rangle^{1/2}$) in the N-body simulations. The main features of $\langle v_{12}^2(r) \rangle^{1/2}$ are (a) monotonic rise at small r ; (b) saturation at large r ; (c) a maximum at medium r . In Section 2.5.1 we will discuss how these features can be explained by some physical arguments. Based on these arguments, we give (in Section 2.5.2) an empirical fitting formula for $\langle v_{12}^2(r) \rangle^{1/2}$, so that it can be calculated easily for any given power spectrum. Readers who are mainly interested in using the model to calculate $\langle v_{12}^2(r) \rangle^{1/2}$ can skip Section 2.5.1 and go directly to Section 2.5.2.

2.5.1. Behaviour of the pairwise peculiar velocity dispersion

At large separations where the correlated motion of particle pairs is negligible, the pairwise peculiar velocity dispersion is

$$\langle v_{12}^2(r \rightarrow \infty) \rangle = \frac{2}{3} \langle v_1^2 \rangle. \quad (15)$$

Thus, the asymptotic value of $\langle v_{12}^2(r) \rangle$ is fixed at a constant for large pair separations.

For very small separations, the main contribution to the pairwise velocity dispersion comes from particle pairs in virialized dark matter haloes (e.g. Marzke et al. 1994; Sheth 1996; Sheth & Jain 1996). Assuming that dark haloes are spherically symmetric and that the velocities of particles in them are isotropic, we can write

$$\langle v_{12}^2(r) \rangle = \frac{1}{3} \langle S^2(|\mathbf{x}|) + S^2(|\mathbf{x} + \mathbf{r}|) \rangle, \quad (16)$$

where $S(r)$ is the 3D velocity dispersion of particles at a radius r from a halo, and $\langle \dots \rangle$ denotes the pair-weighted average over all haloes. Thus, in order to obtain $\langle v_{12}^2(r) \rangle$ defined in equation (16), we need the density profile, as well as the mass function, of dark haloes.

The results of N-body simulations (Hernquist 1990; Navarro, Frenk & White 1996, hereafter NFW; Torman et al. 1996) suggest to write the density and velocity-dispersion profiles as

$$n(r) = n_0 F(r/r_s), \quad (17)$$

$$S^2(r) = S_0^2(r_s) G(r/r_s), \quad (18)$$

where r_s is a scale radius. For simplicity, we assume that the velocity dispersion $S(r)$ at a radius r is $\sqrt{3/2}$ times the circular velocity at that radius, $S^2(r) = (3/2)GM(r)/r$, where $M(r)$ is the mass interior to r . Under such assumption $G(x)$ is determined by $F(x)$,

$$G(x) = \frac{1}{x} \int_0^x F(x) x^2 dx. \quad (19)$$

The total number of pairs of separation r in a halo can then be written as

$$\mathcal{P}(r) dr = 8\pi^2 n_0^2 r_s^3 r^2 dr \int_0^\infty x_1^2 dx_1 F(x_1) \int_{-1}^1 F(x_2) d\beta, \quad (20)$$

where

$$x_2^2 = x_1^2 + (r/r_s)^2 - 2x_1(r/r_s)\beta.$$

Similarly, the S^2 -weighted number of pairs in a halo is

$$\mathcal{P}_S(r) dr = 8\pi^2 n_0^2 r_s^3 S_0^2(r_s) r^2 dr \int_0^\infty x_1^2 dx_1 F(x_1) \int_{-1}^1 F(x_2) [G(x_1) + G(x_2)] d\beta. \quad (21)$$

In carrying out the integrations in equations (20) and (21), we take $F(r/r_s) = 0$ when r is larger than the virial radius of the halo, r_v [which is defined as the radius of the mass shell that encloses the halo mass and settles at about half of its maximum expansion radius, see e.g. Lahav et al. (1991) for more detailed discussion].

We use the Press-Schechter formalism (Press & Schechter 1974) to calculate the mass function of dark haloes. In this formalism, the comoving number density of dark haloes with mass in the range $M \rightarrow M + dM$ is

$$N(M)dM = - \left(\frac{2}{\pi}\right)^{1/2} \frac{\bar{\rho}}{M} \frac{\delta_c}{\sigma(R)} \frac{d \ln \sigma(R)}{d \ln M} \exp \left[-\frac{\delta_c^2}{2\sigma^2(R)} \right] \frac{dM}{M}, \quad (22)$$

where M is the mass of the halo. M is related to the initial comoving radius R of the region from which the halo formed (measured in current units) by $M = \frac{4\pi}{3} \bar{\rho} R^3$, δ_c is the threshold overdensity for collapsing. The predictions of equation (22) have been tested extensively by N-body simulations for various cosmogonies (e.g. Lacey & Coles 1994; Mo, Jing & White 1996).

With the above discussion, we can now write the pairwise velocity dispersion defined in equation (16) as:

$$\langle v_{12}^2(r) \rangle = \frac{1}{3} \frac{\int_0^\infty N(M) \mathcal{P}_S(r) dM}{\int_0^\infty N(M) \mathcal{P}(r) dM}. \quad (23)$$

To complete the description, we need a model for δ_c and the relation between the mass of a halo M and its virial radius r_v . For the values of δ_c in various cosmologies, we take the result summarized in Kochanek (1995; see also Bartelmann et al. 1993). For the relation between r_v and M , we use the formulae given in Lahav et al. (1991). Thus, when r_s and the density profile $F(r/r_s)$ are given, we can easily obtain $\langle v_{12}^2(r) \rangle$ defined in equation (23).

In this paper we will use the model of NFW for the density profile of dark haloes:

$$F(x) = \frac{1}{x(1+x)^2}; \quad (24)$$

$$\delta_0 \equiv \frac{mn_0}{\rho_{\text{crit}}} = \frac{200}{3} \left[\ln(1+c) + (1+c)^{-1} - 1 \right]^{-1} c^3, \quad (25)$$

where ρ_{crit} is the current value of the critical density, m is the mass of a particle and c is the concentration factor,

$$c \equiv \frac{r_{200}}{r_s}, \quad (26)$$

with r_{200} being the radius within which the average mass overdensity of the halo is 200. It should be pointed out that r_{200} is in general different from the virial radius r_v , but for a given density profile the relation between r_v and r_{200} is fixed. The exact value of c for a

halo depends on its formation history and cosmology. The simulation result of NFW shows that $c \sim 5$ -10 for typical haloes [i.e. those with Lagrangian radius $R \sim R_*$ where R_* is defined by $\sigma(R_*) = 1.69$] in the standard CDM model. NFW also proposed a simple model for c based on halo formation time. The formation redshift z_f of a halo identified at redshift $z < z_f$ with mass M is defined as the redshift by which half of its mass is in progenitors with mass exceeding fM , where $f < 1$ is a constant. According to the formula given by Lacey & Cole (1993) based on the Press-Schechter formalism, the halo formation time is then defined implicitly by

$$\text{erfc} \left[\frac{(\delta_{z_f} - \delta_z)}{\sqrt{2[\sigma^2(fM) - \sigma^2(M)]}} \right] = \frac{1}{2}, \quad (27)$$

where δ_z is the threshold overdensity for collapsing at redshift z [e.g. $\delta_z = (1+z)\delta_c$ in an Einstein-de Sitter universe], $\sigma(M)$ is the rms of the linear power spectrum at redshift $z = 0$ in top-hat windows enclosing mass M (see equation 2). NFW have used M_{200} (the mass enclosed in r_{200}) instead of M in equation (27). We will follow their convention. NFW suggested that the characteristic overdensity of a halo identified at redshift z with mass M is related to its formation redshift z_f by

$$\delta_0(M, f, z) = C(f)\Omega_0 [1 + z_f(M, f, z)]^3, \quad (28)$$

where the normalization $C(f)$ depends on f . We will take $f = 0.01$ as suggested by the N-body results of NFW. In this case $C(f) \approx 2 \times 10^3$ (NFW). Thus for a halo of given mass, one can obtain the concentration factor c from equations (25)-(28). In practice, we first solve z_f from equation (27) and insert the value of z_f into equation (28) to get δ_0 , we then use this value of δ_0 in equation (25) to solve for c . As shown by NFW, the value of c does not depend sensitively on the choice of f , as long as $f \ll 0.1$. It is necessary to point out that the arguments given in NFW are originally only for Einstein-de Sitter universe. Fortunately, these arguments are equally valid for low- Ω universes, as is shown recently by Navarro et al. (1996, in preparation).

The dotted lines in Fig.3 show $\langle v_{12}^2(r) \rangle$ given by equation (23) as a function of r . The pairwise velocity dispersion $\langle v_{12}^2(r) \rangle$ increases with r , because for large r the fraction of pairs from big haloes is larger. To examine the sensitivity of our results to the choice of the model for the concentration factor c , we also made calculations for the SCDM models by assuming $c = 5$ and 10. The results are shown in Figs. 3a and 3b as the dashed curves (how these curves are obtained will become clear in the following). A larger value of c gives higher amplitudes for $\langle v_{12}^2(r) \rangle$, because an increase of c enhances the velocity dispersion of a halo in the central region.

It is clear that model (23) will break down for large r where the number of pairs within virialized haloes becomes smaller than other kinds of pairs (e.g. cross pairs between halo particles and field particles, and pairs among field particles). At some separation, the value of $\langle v_{12}^2 \rangle$ should decrease with r and approach the asymptotic value given by equation (15). Although the function $\langle v_{12}^2(r) \rangle$ in the medium range of r is complicated, (because it depends not only on the amplitude but also on the shape of the three-point correlation functions, see below), it may still be possible to find some physically motivated models to understand the features observed in the simulations, given the asymptotic behaviour of $\langle v_{12}^2(r) \rangle$ on both small and large separations.

We start with equation (72.1) in Peebles (1980):

$$\begin{aligned} & \frac{\partial}{\partial t} (1 + \xi) v^\alpha + \frac{\dot{a}}{a} (1 + \xi) v^\alpha + \frac{1}{a} \frac{\partial}{\partial x^\beta} (1 + \xi) \langle v_{12}^\alpha v_{12}^\beta \rangle \\ & + \frac{2Gm}{a^2} \frac{x^\alpha}{x^3} (1 + \xi) + 2G\bar{\rho}a \frac{x^\alpha}{x^3} \int_0^x d^3x \xi + 2G\bar{\rho}a \int d^3x_3 \zeta(1, 2, 3) \frac{x_{13}^\alpha}{x_{13}^3} = 0, \end{aligned} \quad (29)$$

where $v^\alpha = \langle v_{12}^\alpha \rangle$ is the α -component of the mean pairwise peculiar velocity (see equation 10a), $\zeta(1, 2, 3)$ is the three point correlation function, m is the mass of a particle. The fourth term describes the mutual attraction of the particle pair and can be neglected when we consider dark matter particles. We write the velocity dispersion as

$$\langle v_{12}^\alpha v_{12}^\beta \rangle = \left[\frac{2}{3} \langle v_1^2 \rangle + \Sigma \right] \delta_{\alpha\beta} + [\Pi - \Sigma] \frac{x^\alpha x^\beta}{x^2}, \quad (30)$$

where $\langle v_1^2 \rangle$ is the mean square peculiar velocity of particles (equation 11), Π and Σ represent the effects of the correlated motions on the components of the dispersion parallel and perpendicular to the separation. Thus the (1D) velocity dispersion defined in the beginning of this subsection is $\langle v_{12}^2(r) \rangle = \frac{2}{3} \langle v_1^2 \rangle + \Pi$. Using the boundary condition that $\xi(r \rightarrow \infty) = 0$ and $\Pi(r \rightarrow \infty) = 0$ (see Peebles 1980, §72), we can obtain a formal solution for $\langle v_{12}^2(r) \rangle$ from equation (29):

$$\begin{aligned} [1 + \xi(r)] \langle v_{12}^2(r) \rangle &= \frac{2}{3} \langle v_1^2 \rangle + 3\Omega(Hr)^2 I - (Hr)^2 \left[\frac{\partial^2 I}{\partial (\ln a)^2} + \frac{\partial I}{\partial \ln a} \frac{\partial \ln H}{\partial \ln a} + 2 \frac{\partial I}{\partial \ln a} \right] \\ &+ 2 \int_r^\infty \frac{dr}{r} [1 + \xi(r)] (\Pi - \Sigma) + \frac{3\Omega H^2}{4\pi} \int_r^\infty \frac{dr}{r} \int d^3q \frac{\mathbf{r} \cdot \mathbf{q}}{q^3} \zeta(r, q, |\mathbf{r} - \mathbf{q}|), \end{aligned} \quad (31)$$

where

$$I \equiv \int_0^\infty \frac{dk}{k} \Delta_E^2(k, a) \frac{\sin kx}{(kx)^3}. \quad (32)$$

Note that r in equation (31) is the physical radius. Since models for ξ , $\langle v_1^2 \rangle$ and Δ_E have already been constructed, we need only to specify $\Pi - \Sigma$ and the integration of ζ in the last term of equation (31) to complete our model for $\langle v_{12}^2(r) \rangle$.

For our demonstration, we will assume that the three point correlation function ζ on small scales obeys the hierarchical form:

$$\zeta(r_1, r_2, r_3) = Q [\xi(r_1)\xi(r_2) + \xi(r_2)\xi(r_3) + \xi(r_3)\xi(r_1)], \quad (33)$$

where Q is a constant. It is clear from equation (31) that the pairwise peculiar velocity dispersion on small scales is dominated by the term of the three point correlation. In this case, we can write

$$\langle v_{12}^2(r) \rangle = \frac{3\Omega H^2 Q}{4\pi[1 + \xi(r)]} \int_r^\infty \frac{dr}{r} \int d^3q \frac{\mathbf{r} \cdot \mathbf{q}}{q^3} [\xi(r)\xi(q) + \xi(q)\xi(|\mathbf{r} - \mathbf{q}|) + \xi(|\mathbf{r} - \mathbf{q}|)\xi(r)]. \quad (34)$$

Since ξ is known for a given model (see §2.2), the value of Q can then be determined by specifying $\langle v_{12}^2(r) \rangle$ at some small fiducial radius r_Q . On using our model for $\langle v_{12}^2(r) \rangle$ on small scales, the last term of equation (31) can therefore be fixed, as long as the hierarchical form (33) holds. On small scale, the hierarchical form is a reasonable approximation, however on large scales, Q is not a constant but depends on the size and shape of the triangle specified by (r_1, r_2, r_3) (see e.g. Matsubara & Suto 1994; Jing & Börner 1996). Unfortunately, a theoretical model is not yet available to describe Q as a function of (r_1, r_2, r_3) ¹. In what follows, we assume equation (33) to hold on all scales. We will show that the error in $\langle v_{12}^2(r) \rangle$ caused by such an assumption can be corrected by a simple model.

To model $\Pi - \Sigma$, we define a quantity which describes the anisotropy of the relative peculiar velocity dispersion:

$$\mathcal{A}(r) \equiv 1 - \frac{\frac{2}{3}\langle v_1^2 \rangle + \Sigma(r)}{\langle v_{12}^2(r) \rangle}. \quad (35a)$$

It then follows that

$$\Pi - \Sigma = \mathcal{A}(r)\langle v_{12}^2(r) \rangle. \quad (35b)$$

On small scales where the velocity dispersion is isotropic, we have $\mathcal{A} = 0$. On large scales where linear theory applies, we can write (see Peebles 1993, §21, note also the slight difference in the definitions of Π and Σ):

$$\Pi(r) = -\frac{2}{3} \left(\frac{\dot{D}}{D} \right)^2 \left[\frac{J_5(r)}{r^3} + K_2(r) \right]; \quad (36a)$$

$$\Sigma(r) = -\left(\frac{\dot{D}}{D} \right)^2 \left[\frac{J_3(r)}{r} - \frac{J_5(r)}{3r^3} + \frac{2}{3}K_2(r) \right], \quad (36b)$$

¹Note that the relevant quantity in our problem is the integration of ζ in the last term of equation (31), which is only a one-dimensional function of r and should therefore be much easier to model than ζ itself.

where

$$J_3(r) = \int_0^r r^2 \xi(r) dr = r^3 \int_0^\infty \frac{dk}{k} \frac{\Delta^2(k)}{(kr)^3} (\sin kr - kr \cos kr);$$

$$J_5(r) = \int_0^r r^2 \xi(r) dr = r^5 \int_0^\infty \frac{dk}{k} \frac{\Delta^2(k)}{(kr)^5} \left\{ kr [6 - (kr)^2] \cos kr + 3 [(kr)^2 - 2] \sin kr \right\};$$

$$K_2(r) = \int_r^\infty r \xi(r) dr = r^2 \int_0^\infty \frac{dk}{k} \frac{\Delta^2(k)}{(kr)^2} \cos kr.$$

In the above equations, $\Delta^2(k)$ is the dimensionless power spectrum in the linear regime. We will, however, insert the nonlinear power spectrum so that some nonlinear effects can be taken into account. Figure 5 compares \mathcal{A} predicted by equations (35) and (36) (solid curves) to that derived from the simulations. The overall anisotropy in the velocity dispersion is quite small, and on separations $r \gtrsim 2 h^{-1} \text{Mpc}$ it is reasonably well described by our model. Since the $(\Pi - \Sigma)$ term is expected to be important only on large scales, we will use equation (36) to estimate $(\Pi - \Sigma)$.

The dot-dashed curves in Fig.3 show the pairwise peculiar velocity dispersion $\langle v_{12}^2(r) \rangle^{1/2}$ given by equation (31) with the assumptions discussed above. We have taken $r_Q = 0.1 h^{-1} \text{Mpc}$. As one can see from the figure, the result is not sensitive to the exact value of r_Q , as long as r_Q is small. Our model successfully gives a maximum in $\langle v_{12}^2(r) \rangle^{1/2}$, as observed in the N-body simulations. The maximum occurs at a separation characteristic of the size of typical clusters, about $1\text{--}2 h^{-1} \text{Mpc}$. This happens because most particles forming pairs of larger separations are in low-density environments where the velocity dispersion is low. The model overestimates the pairwise peculiar velocity dispersion on large scales when compared to the results derived from the N-body simulations (shown by the symbols). This overestimation comes mainly from our assumption that Q is a constant. Indeed, the value of Q may decrease substantially on large scales, as shown by N-body simulations (e.g. Jing & Börner 1996). The contribution to $\langle v_{12}^2(r) \rangle$ from the three-point correlation is therefore overestimated on large scales in our model. As discussed above, a reliable model for ζ over different scales is still lacking at present time, and we have to invoke some simple arguments to correct the errors caused by the assumption of equation (33).

As we have discussed above, for small separations r , most pairs are in virialized haloes and equation (33) should be a reasonable description. The assumption of equation (33) fails for large r , because pairs outside dark haloes become important. As the simplest choice, the fraction of particles in dark haloes with radius $r_{200} \geq \alpha_h r$ (α_h being a constant), $f_h(\alpha_h r)$, may be a good guess of the function that controls the change of $\langle v_{12}^2(r) \rangle$ from its small separation value to its large separation value. According to the Press-Schechter formalism

(see equation [22]), $f_h(\alpha_h r)$ can be written in terms of the initial power spectrum as:

$$f_h(\alpha_h r) = \text{erfc} \left[\frac{\delta_c}{\sqrt{2}\sigma(R_h)} \right], \quad (37)$$

where R_h is the linear radius of a halo with $r_{200} = \alpha_h r$. Thus when r is very small, all particles are in haloes so that $f_h = 1$, while $f_h = 0$ when $r \rightarrow \infty$. This behaviour of f_h suggests the following empirical formula for $\langle v_{12}^2(r) \rangle$:

$$\langle v_{12}^2(r) \rangle = [f_h(\alpha_h r)]^\tau \langle v_{12}^2(r) \rangle_s + \{1 - [f_h(\alpha_h r)]^\tau\} \times \frac{2}{3} \langle v_1^2 \rangle, \quad (38)$$

where we have changed our notation so that $\langle v_{12}^2(r) \rangle_s$ denotes the $\langle v_{12}^2(r) \rangle$ defined by equation (31). The values of α_h and τ are to be calibrated by results from N-body simulations.

The thick solid curve in Figure 3a is calculated according to (38) with the values

$$\alpha_h = 0.2; \quad \tau = 1. \quad (39)$$

It is clear that the model fits the simulation results for the SCDM model with $\sigma_8 = 0.62$ reasonably well. The predictions of $\langle v_{12}^2(r) \rangle$ for other cosmogonical models are shown by the thick curves in the other panels of Fig.3, using the same values of α_h and τ as given in equation (39). The figure shows that our model also works for these cosmogonies. For comparison, the two dashed curves in Figs. 3a and 3b show the same results obtained by assuming the concentration factor $c = 5$ (lower curve) and 10.

The good agreement between the model predictions and the N-body results shows that the main features in $\langle v_{12}^2(r) \rangle$ can indeed be explained by our simple physical considerations.

2.5.2. Fitting formula for the pairwise peculiar velocity dispersion

The model for $\langle v_{12}^2(r) \rangle$ given in Section 2.5.1, although having physical motivations, is not easy to implement. In this section we provide a much simpler fitting formula for $\langle v_{12}^2(r) \rangle^{1/2}$.

Based on the N-body results and the discussion in Section 2.5.1 we make the following ansatz for $\langle v_{12}^2(r) \rangle$:

$$\langle v_{12}^2(r) \rangle^{1/2} = \Omega^{0.5} H r_c \phi(r/r_c), \quad (40a)$$

where $\phi(x)$ is a universal function and r_c is a nonlinear scale. We choose r_c to be the virial radius of M^* haloes, r_v^* . For a given power spectrum, the linear radius of M^* haloes, r_0^* , is

given by $\sigma(r_0^*) = 1$. The relation between r_v^* and r_0^* in different cosmological models can be obtained by using the formulae given in Appendix B. We approximate the functional form of $\phi(x)$ by:

$$\phi(x) = \frac{\phi_\infty(1 + Bx^{-\beta}) + Ax^{-\alpha}}{1 + V[g(a)]^{0.35}[\Omega(a)]^{0.2}x^{-(\alpha+\epsilon)}}, \quad (40b)$$

where $\phi_\infty = \sqrt{\frac{2}{3}}\langle v_1^2 \rangle^{1/2}/(Hr_c\Omega^{0.5})$; $A, B, V, \alpha > \beta > 0$, and $\epsilon > 0$ are constant. It follows that for $r \rightarrow \infty$, $\langle v_{12}^2(r) \rangle$ is forced to have the asymptotic value given by equation (15). For $r \rightarrow 0$, $\langle v_{12}^2(r) \rangle^{1/2} \propto x^\epsilon$ so that it increases with r as a power law. The dependence on the linear growth factor $g(a)$ is included to take into account the fact that for a given power spectrum, haloes with the same linear radius may have different density profiles (or concentrations) in different cosmological models (see Section 2.5.1). The power of $g(a)$ can be fixed by comparing the amplitudes of $\langle v_{12}^2(r) \rangle^{1/2}$ at small r for models (having the same initial power spectrum) with or without a cosmological constant. We found that a value of about 0.35 gives a reasonably good fit to our N-body results. The dependence on Ω is included because for a given virial radius of a halo the ratio $S/\Omega^{0.5}$ (where S is the velocity dispersion of the halo) is larger in a lower-density universe.

The solid curves in Fig.4 show the predictions of our fitting formula with

$$A = 58.67; \quad B = -0.3770; \quad V = 4.434; \quad (40c)$$

$$\alpha = 2.25; \quad \beta = 1.90; \quad \epsilon = 0.15. \quad (40d)$$

It is clear that the formula gives a reasonably good fit to all cosmogonical models examined in the present paper. At the moment, it is not clear whether the small discrepancy (typically $\lesssim 20$ percent) between the model predictions and simulation results in some cases is due to the inaccuracy of our model, or due to the lower resolution of our simulations, or due to both of them. As one can see from Fig.4a, a lower resolution indeed reduces the pairwise peculiar velocity dispersion. Obviously, better simulations are needed to give a more accurate calibration of our formula. Given the uncertainties in our present simulations, we do not intend to obtain the best fit values for the parameters in equation (40b).

2.6. The Hierarchical Amplitude of the Three-Point Correlation Function

Given the model for $\langle v_{12}^2(r) \rangle$, we can use equation (34) to calculate the hierarchical amplitude Q on small scales. In Figure 6 the solid curves show Q as a function of r predicted by our fitting formula (40). The amplitude Q decreases only slowly with r for $r \sim 0.1 h^{-1}\text{Mpc}$, showing that equation (33) is valid on small scales. The symbols in the figure show the values of Q estimated from N-body simulations by averaging over all triplets

with the smallest side equal to r and with the second smallest side less than $4r$. Thus this quantity is *not* exactly the same as the one given by the model. However, since for small r the value of Q does not depend strongly on the shape of the triplets (see Jing 1996, in preparation), the comparison between the model and the simulation results may still be meaningful. The figure shows that our model prediction is generally in agreement with the simulation results. The values of Q at small separations ($r \sim 1 h^{-1}\text{Mpc}$) are typically 1-2, without a strong dependence on cosmogonies. These values of Q are only slightly larger than those obtained for galaxies ($Q \sim 1$ for optical galaxies, see e.g. Groth & Peebles 1977; Jing, Mo & Börner 1991).

If the cosmic virial theorem is used under the assumptions that the two-point correlation function has a power-law form, $\xi(r) = A_0 r^{-\gamma}$, and that the three-point correlation function ζ has the hierarchical form given by equation (33), then the pairwise velocity dispersion on small scales can be written as:

$$\langle v_{12}^2(r) \rangle = \frac{2\pi G \bar{\rho} Q A_0 r^{2-\gamma} J(\gamma)}{(\gamma - 1)(2 - \gamma)(4 - \gamma)} \quad (41)$$

(see Peebles 1980, Section 75). Here

$$J(\gamma) = \int_0^\infty dy y^{-2} (1 + y^{-\gamma}) \mathcal{M}$$

with

$$\mathcal{M} = (1 + y)^{2-\gamma} [1 - (2 - \gamma)y + y^2] - |1 - y|^{2-\gamma} [1 + (2 - \gamma)y + y^2].$$

Thus, by using our model for $\langle v_{12}^2(r) \rangle$ and by fitting $\xi(r)$ to a power law on small scales to get A_0 , we can also get the value of Q from equation (41). The validity of equation (41) was checked by Suto (1993) using N-body simulations. There is, however, an uncertainty here. As one can see from Fig.1, $\xi(r)$ is not a good power-law even on small scales, the value of γ determined from ξ depends therefore on the range of r used in the fitting. Indeed, for $r \sim 1 h^{-1}\text{Mpc}$, the local value of γ can sometimes be larger than 2 and equation (41) is ill-defined. Since it is unclear which range of r is most relevant for $\langle v_{12}^2(r) \rangle$ on small scales, it does not seem to be a good idea to use γ obtained from ξ in equation (41) to obtain Q . Fortunately, the value of γ in equation (41) can also be determined from the dependence of $\langle v_{12}^2(r) \rangle$ on r . On small scales, $\langle v_{12}^2(r) \rangle$ increases with r approximately as a power law (Fig.4). Thus the value of γ given by fitting $\langle v_{12}^2(r) \rangle$ to a power law is always smaller than 2, and equation (41) is well defined. The value of the correlation amplitude, A_0 , can still be determined reasonably well by fitting $\xi(r)$ on small scales to a power law. As one can see from equation (41), the error in Q induced by A_0 is only proportional to that in A_0 . In Table 2, we show the values of Q predicted by equations (40) and (41) for $\xi(r)$ and $\langle v_{12}^2(r) \rangle$ in the range $r = 0.1 - 0.5 h^{-1}\text{Mpc}$, along with the values of γ obtained by fitting $\langle v_{12}^2(r) \rangle$ to a power law. The values of Q obtained in this way are similar to those shown in Fig.6.

3. THE EFFECT OF REMOVING MASSIVE HALOES ON $\langle v_{12}^2(r) \rangle$

Davis & Peebles (1983) have calculated the pairwise velocity dispersion of galaxies for the CfA1 redshift survey (Huchra et al. 1983). Their result, $\langle v_{12}^2(r) \rangle^{1/2} = 340 \pm 40 \text{ km s}^{-1}$, had been used for about 10 years to judge models of structure formation, and was a primary argument against the CDM model with $\Omega_0 = 1$ and with $\sigma_8 \sim 1$. Based on the same data set, Mo, Jing & Börner (1993, see also Zurek et al. 1994; Somerville, Davis & Primack 1996) found that this statistic is sensitive to the presence (or absence) of galaxy clusters in a sample, and the constraint given by the observational results is uncertain. Recently, similar analyses have been performed on new, larger redshift surveys (Fisher et al. 1994; Guzzo et al. 1995; Marzke et al. 1995), but the problem remains: there is a large variation in $\langle v_{12}^2(r) \rangle$ between different surveys, and even for the same survey analysed in different ways. From our model for $\langle v_{12}^2(r) \rangle$ (see Section 2.5.1), we see clearly why the observed small scale pairwise velocity dispersion is sensitive to the presence (or absence) of galaxy clusters. Indeed, from equations (20)-(23) we can write

$$\langle v_{12}^2(r) \rangle \propto \frac{\int_0^\infty N(M) M^{5/3} dM}{\int_0^\infty N(M) M dM}, \quad (42)$$

where we have assumed that $M \propto r_s^3$ and $S_0^2 \propto M^{2/3}$. These assumptions are approximately correct for haloes with density profiles close to isothermal. Using equation (22) we see that while the number of pairs with small separations is dominated by dark haloes with $M \sim M_*$ (where M_* is the mass at which the rms mass fluctuation $\sigma = 1$), the pairwise peculiar velocity dispersion on small scale can be significantly affected by massive ones with $M > M_*$. The number density of such massive haloes is small and a large sample is therefore needed to have a fair sampling of their number density. Marzke et al. (1995) have discussed in considerable detail how such sampling can affect the statistics on $\langle v_{12}^2(r) \rangle$. In this paper, we will not discuss this effect in detail. Instead, we show that from our model one can derive some new statistics which may be more robust against the sampling effect discussed above.

Somerville, Primack & Nolthenius (1996) have suggested that studying $\langle v_{12}^2(r) \rangle$ as clusters (dark haloes) with different internal velocity dispersions are removed leads to interesting information about the amount of power on cluster and subcluster scales. Since in practice the internal velocity dispersions of dark haloes are not easy to measure accurately for a large number of haloes, we suggest to study $\langle v_{12}^2(r) \rangle$ as a function of the mean separation of the clusters that are removed from the analysis.

From equation (22), we can write the total comoving number density of haloes with

mass exceeding M as

$$N(> M) = -\frac{3}{(2\pi)^{3/2}} \int_R^\infty \frac{1}{R^3} \frac{\delta_c}{\sigma(R)} \frac{d \ln \sigma}{d \ln R} \exp \left[-\frac{\delta_c^2}{2\sigma^2} \right] \frac{dR}{R}. \quad (43)$$

The mean separation of haloes with mass exceeding M is therefore $\bar{d}(M) \equiv [N(> M)]^{-1/3}$. As one can see from equation (43), for a given power spectrum, \bar{d} determines R . Thus the effect of removing haloes with masses exceeding M in the model is to change the upper limits of the integrations in equation (23) from ∞ to M . This obviously has the effect of reducing $\langle v_{12}^2(r) \rangle$ on small scales. In Figure 7 we show $\langle v_{12}^2(r) \rangle^{1/2}$ at $r = 0.1 h^{-1} \text{Mpc}$ as a function of \bar{d} for the SCDM models ($\Gamma = 0.5$) with $\sigma_8 = 0.62$ and 1.24 , and for three other cosmogonical models with $\Gamma = 0.2$ and $\sigma_8 \Omega_0^{0.6} = 0.38$. The use of the combination $\sigma_8 \Omega_0^{0.6}$ is motivated by the fact that this quantity can be determined from observations based on large scale velocity fields (see e.g. Dekel 1994, Fisher et al. 1994) and on cluster abundance and clustering (e.g. White, Efstathiou & Frenk 1992; Mo, Jing & White 1996). The specific value 0.38 is chosen simply because the OPEN and FLAT models have this value. The figure shows that the value of $\langle v_{12}^2(r) \rangle^{1/2}$ does not reach its asymptotic value even for $\bar{d} \sim 50 h^{-1} \text{Mpc}$ (the typical value for the mean separation of rich clusters). Thus to have the small scale pairwise peculiar velocity dispersion fairly sampled, one needs a sample that contains many rich clusters. All galaxy redshift samples used so far to derive $\langle v_{12}^2(r) \rangle$ are not large enough to qualify for this purpose, and it is not surprising that the values of the small scale pairwise peculiar velocity dispersion of galaxies derived from available galaxy samples are uncertain.

However, by inspecting Fig.7 we see that some useful statistics based on the pairwise velocity dispersion can still be derived from relatively small samples. For a given sample, we first identify from it clusters (groups) of different masses. We then remove successively the most massive clusters from the sample and analyze the small scale pairwise peculiar velocities as a function of the mean separation of clusters (\bar{d}) that have been removed from the sample. Given a small sample, such a function can be determined reliably only for small values of \bar{d} , because the mass function is well sampled only for relatively poor clusters. As one can see from Fig.7, the model prediction for this function is quite different for different cosmogonies.

Another interesting point to note from Fig.7 is the difference in the results for the OPEN, FLAT and the ($\Omega_0 = 1, \Gamma = 0.2, \sigma_8 = 0.38$) model. All these three models have the same shape of the power spectrum ($\Gamma = 0.2$) and the same value of $\sigma_8 \Omega_0^{0.6}$ ($= 0.38$). As we have discussed before, it is difficult to determine Ω_0 and σ_8 separately from observations on large scale velocity fields or on cluster abundance. On the other hand, it is relatively easy to determine the combination $\sigma_8 \Omega_0^{0.6}$ from these observations. Fig.7 shows, however,

that one can hope to separate Ω_0 and σ_8 by measuring the small scale peculiar velocity dispersion. The small scale pairwise peculiar velocity dispersion is lower in the model with $\Omega_0 = 1$ than in the OPEN and FLAT models with the same $\sigma_8\Omega_0^{0.6}$, because clusters in this model formed late and thus are less concentrated. For the same reason, the small scale pairwise peculiar velocity dispersion is lower in the FLAT model than in the OPEN model. This line of argument is obviously worth further investigation.

4. DISCUSSION

The analytical models presented in Section 2 allow us to see clearly how the low order statistics of the density and the velocity distributions are determined by cosmological model and initial power spectrum. As a result we can use them to construct some statistical measures of the density and peculiar velocity fields to constrain models by observations. In this Section we will briefly discuss several possible applications of our results. Details of these applications will be described elsewhere.

As a first application our results can be used to construct models for the reconstruction of cosmogonical parameters from measurements in redshift space. As discussed in Fisher et al. (1994, and references therein), in order to use the redshift-space distortion on the two-point correlation function to derive cosmological parameters, it is necessary to model the distribution of the pairwise peculiar velocity. The distribution function is usually constructed from the low-order statistics of the pairwise peculiar velocity, which, by using our model, can all be calculated directly for any given cosmogony. Thus a likelihood function can be written for the pairwise peculiar velocities, which depends only on the cosmogonical parameters. Given a redshift sample of galaxies, one can then hope to constrain the cosmogonical parameters by maximizing the likelihood function.

A second application of our models is to use them to examine what happens to some statistics, if the power spectrum is filtered in some manner. Such an investigation is important, because (1) real observations do not sample all parts of the spectrum equally well, and we need to understand how such sampling affects our statistics; and (2) we may sometimes want to filter the density field deliberately in order to get some insight into the underlying density field. In Section 3 we have already shown one such example related to the effect of removing massive clusters on the values of the pairwise peculiar velocity dispersions on small scales. Here we give another one.

The mean square velocity $\langle v_1^2 \rangle$ given by the cosmic energy equation presented in Subsection 2.4 contains both large scale bulk motion and small scale random motion. It is

sometimes desirable to separate these two kinds of motions by filtering the mass density spectrum. From equation (13), one can have a ‘filtered version’ of the cosmic energy equation:

$$\langle v_1^2(x) \rangle = \frac{3}{2} \Omega H^2 a^2 \left[I_2(x, a) - \frac{1}{a} \int_0^a I_2(x, a) da \right], \quad (44)$$

where

$$I_2(x, a) = \int_0^\infty \frac{dk}{k} \frac{\Delta_E^2(k, a)}{k^2} W(k; x) \quad (45)$$

with $W(k; x)$ being a filter with characteristic (comoving) radius of x . It is clear from equation (45) that if the high-frequency modes are filtered out from the dimensionless power spectrum Δ_E^2 , then the velocity defined by equation (44) describes the motions induced by the low-frequency modes of the density perturbations. In linear case, this is just the mean square of the bulk motion of dark matter in the filter. On the other hand, if low frequency modes are filtered out, the velocity defined by equation (44) describes small scale relative motions. The statistics of the filtered velocity field can be derived either from velocity data (e.g. those based on Tully-Fisher relations) or from redshift-space distortions (see Miller, Davis & White 1996 for a discussion). Our model will then provide a clear picture how cosmogonical models are constrained by these measurements.

It must be pointed out once again that in order to make any rigorous comparison between models and observations of galaxy distribution we need to understand how galaxy distribution is related to dark matter distribution. Much work needs to be done in this respect. However, for a given cosmogonical model, the density bias parameter, defined by the ratio between the two-point correlation function of galaxies and that of mass, and the velocity bias parameter, defined by *e.g.* the ratio between the pairwise peculiar velocity dispersion of galaxies and that of dark matter, are actually fixed. Our model can therefore be used to understand the effects of biased galaxy formation on the low-order moments of galaxy distribution with respect to those of dark matter.

Finally, it is necessary to point out that the accuracy of our analytical models depends on the accuracy of the N-body simulations used to calibrate them. At present time, the discrepancy between our analytical formulae and simulation results is typically 20 percent. It is still unclear whether this small but significant discrepancy results from the inaccuracy of our analytical models, or from the limited resolution of N-body simulation, or from both of them. However, the method described in our paper is general. With improved N-body simulations, the fitting formulae for the evolved power spectrum and for the halo density profiles can all be improved. More accurate models for the low-order moments of dark matter distribution can then be easily obtained by using the procedure outlined in our paper.

We thank John Peacock, our referee, for a very useful report. We also thank Julio Navarro, Yasushi Suto, David Syer and Simon White for helpful discussions. The simulation data was generated when YPJ held an Alexander-von-Humboldt research fellowship. This work was also supported by SFB375.

REFERENCES

- Bardeen J., Bond J.R., Kaiser N., Szalay A.S., 1986, *ApJ*, 304
- Bartelmann M., Ehlers J. & Schneider P., 1993, *A&A*, 280, 351
- Carroll S.M., Press W.H., Turner E.L., 1992, *ARAA*, 30, 499
- Davis M., Peebles P.J.E., 1983, *ApJ*, 267, 465
- Dedel A., 1994, *ARAA*, 32, 371
- Efstathiou G., Bond J.R., White S.D.M., 1992, *MNRAS*, 258, 1P
- Fisher K.B., Davis M., Strauss M.A., Yahil A., Huchra J.P., 1994, *MNRAS*, 267, 927
- Groth E.J., Peebles P.J.E., 1977, *ApJ*, 217, 385
- Guzzo L., Fisher K.B., Strauss M.A., Giovanelli R., Haynes M.P., 1995, preprint
- Hamilton A.J.S., Kumar P., Lu E., Matthews A., 1991, *ApJ*, 374, L1
- Hernquist L., 1990, *ApJ*, 356, 359
- Huchra J.P., Davis M., Latham D.W., Tonry J., 1983, *ApJS*, 52, 89
- Jain B., 1996, *MNRAS*, submitted
- Jain B., Mo H.J., White S.D.M., 1995, *MNRAS*, 276, L25
- Jing Y.P., Börner G., 1996, *A&A*, in press
- Jing Y.P., Mo H.J., Börner G., 1991, *A&A*, 252, 449
- Jing Y.P., Mo H.J., Börner G., Fang L.Z., 1995, *MNRAS*, 276, 417
- Kochanek C.S., 1995, *ApJ*, 453, 545
- Lacey C., Cole S., 1993, *MNRAS*, 262, 627
- Lahav O., Lilje P.B., Primack J.R., Rees M.J., 1991, *MNRAS*, 251, 128
- Ma C.P., 1996, *ApJ*, in press
- Marzke R.O., Geller M.J., daCosta L.N., Huchra J.P., 1995, *AJ*, 110, 477
- Matsubara T., Suto Y., 1994, *ApJ*, 420, 497

- Miller A., Davis M., White S.D.M., 1996, preprint
- Mo H.J., Jing Y.P., Börner G., 1993, MNRAS, 264, 825
- Mo H.J., Jing Y.P., White S.D.M., 1996, MNRAS, in press
- Navarro J., Frenk C., White S.D.M., 1996, ApJ, in press (NFW)
- Padmanabhan T., Cen R., Ostriker J.P., Summers F.J., 1996, ApJ, submitted
- Peacock J.A., Dodds S.J., 1994, MNRAS, 267, 1020
- Peacock J.A., Dodds S.J., 1996, MNRAS, 280, L19 (PD)
- Peebles P.J.E., 1980, The Large-Scale Structure of the Universe, Princeton University Press, Princeton
- Peebles P.J.E., 1993, The Principle of Physical Cosmology, Princeton University Press, Princeton
- Press W.H. & Schechter P., 1974, ApJ, 187, 425 (PS)
- Sheth R., 1996, MNRAS, submitted
- Sheth R., Jain B., 1996, MNRAS, submitted
- Somerwille R., Davis M., Primack J.R., 1996, ApJ, submitted
- Somerwille R., Primack J.R., Nolthenius R., 1996, ApJ, submitted
- Suto Y., 1993, Prog. Theor. Phys., 90, 1173
- Tormen G., Bouchet F.R., White S.D.M., 1996, MNRAS, submitted
- Viana P.T.P., Liddle A.R., 1996, MNRAS, in press
- White S.D.M., Efstathiou G., Frenk C., 1993, MNRAS, 262, 1023
- Zurek W., Quinn P.J., Salmon T.K., Warren M.S., 1994, ApJ, 431, 559

A. The Explicit Expression for $\partial\Delta_E^2/\partial a$

From equations (5)-(9) we see that $\Delta_E^2(k, a)$ depends on the expansion factor a through $g(a)$ and $x \equiv \Delta^2(k_L)$, and we can write

$$\left(\frac{\partial\Delta_E^2(k, a)}{\partial a}\right)_k = \frac{\partial f}{\partial g} \frac{dg}{da} + \frac{\partial f}{\partial x} \left(\frac{\partial x}{\partial a}\right)_k. \quad (A1)$$

The linear power spectrum Δ^2 evolves according to the linear theory so that $x = [\mathcal{G}(a)]^2 x_0$, where $\mathcal{G}(a) \equiv [ag(a)/a_0g(a_0)]$ and $x_0 \equiv \Delta^2(k_L, a_0)$ is the linear power spectrum at a fiducial expansion factor a_0 (e.g. at present time). Thus

$$\left(\frac{\partial x}{\partial a}\right)_k = \frac{d\mathcal{G}^2}{da}x_0 + \mathcal{G}^2 \frac{dx_0}{dk_L} \left(\frac{\partial k_L}{\partial a}\right)_k, \quad (\text{A2})$$

where $k_L \equiv [1 + \Delta_E^2(k, a)]^{-1/3}k$. Inserting (A2) into (A1) we have:

$$\left(\frac{\partial \Delta_E^2(k, a)}{\partial a}\right)_k = \left[\frac{\partial f}{\partial g} \frac{dg}{da} + \frac{\partial f}{\partial x} \frac{d\mathcal{G}^2}{da} x_0\right] \left[1 + \frac{\mathcal{G}^2}{3} \left(\frac{k_L}{k}\right)^3 \frac{dx_0}{d \ln k_L} \frac{\partial f}{\partial x}\right]^{-1}. \quad (\text{A3})$$

The derivatives on the right hand side of (A3) are:

$$\frac{dg}{da} = \frac{\partial g}{\partial \Omega} \frac{d\Omega}{da} + \frac{\partial g}{\partial \lambda} \frac{d\lambda}{da}; \quad (\text{A4})$$

$$\frac{d\Omega}{da} = -\frac{\Omega_0(1 - \Omega_0 - \lambda_0 + 3a^2\lambda_0)}{[a + \Omega_0(1 - a) + \lambda_0(a^3 - a)]^2}; \quad (\text{A5})$$

$$\frac{d\lambda}{da} = \frac{a^2\lambda_0[2a(1 - \Omega_0 - \lambda_0) + 3\Omega_0]}{[a + \Omega_0(1 - a) + \lambda_0(a^3 - a)]^2}; \quad (\text{A6})$$

$$\frac{\partial g}{\partial \Omega} = \frac{15\Omega^{4/7}/14 + 5/2 - 69\lambda/28}{[\Omega^{4/7} - \lambda + (1 + \Omega/2)(1 + \lambda/70)]^2}; \quad (\text{A7})$$

$$\frac{\partial g}{\partial \lambda} = \frac{(5\Omega/2)[1 - (1 + \Omega/2)/70]}{[\Omega^{4/7} - \lambda + (1 + \Omega/2)(1 + \lambda/70)]^2}; \quad (\text{A8})$$

$$\frac{d\mathcal{G}^2}{da} = \frac{2\mathcal{G}^2}{a} \left(1 + \frac{d \ln g}{d \ln a}\right); \quad (\text{A9})$$

$$\frac{\partial f}{\partial g} = -\frac{3f}{g} \frac{\mathcal{Q}(x)}{1 + \mathcal{Q}(x)}; \quad (\text{A10})$$

$$\frac{\partial f}{\partial x} = \frac{f}{x} \left[1 + \frac{(1 - \alpha\beta)Bx + \alpha\mathcal{R}(x)}{1 + \mathcal{R}(x)} - \frac{(\alpha - 1/2)\mathcal{Q}(x)}{1 + \mathcal{Q}(x)}\right]. \quad (\text{A11})$$

The quantities in the above equations are defined in Subsection 2.2.

B. The Relation between Linear and Virial Radii of Dark Haloes

As shown by Lahav et al. (1991) the ratio between the virial radius r_v and the turnaround radius r_m of a dark halo can approximately be written as

$$\frac{r_v}{r_m} = \frac{1 - \eta/2}{2 - \eta/2}, \quad (B1)$$

where

$$\eta = 2\lambda_0\Omega_0^{-1}\Xi^{-1}(1 + z_m)^{-3}, \quad (B2)$$

with z_m being the redshift at turnaround and Ξ being the ratio between the halo and background densities at turnaround. The ratio between the linear radius (r_0) and the virial radius (r_v) of a halo can then be written as

$$\frac{r_0}{r_v} = (1 + z_m)\Xi^{1/3}\frac{2 - \eta/2}{1 - \eta/2}. \quad (B3)$$

The value of Ξ depends on z_m as well as on cosmological parameters. Viana & Liddle (1996) gave an accurate fitting formula for Ξ as a function of $\Omega \equiv \Omega(z_m)$:

$$\Xi = \left(\frac{3\pi}{4}\right)^2 \Omega^{-f(\Omega)}, \quad (B4)$$

where

$$f(\Omega) = 0.76 - 0.25\Omega \quad (\text{open universe}); \quad (B5)$$

$$f(\Omega) = 0.73 - 0.23\Omega \quad (\text{flat universe}). \quad (B6)$$

Thus, the relation between r_0 and r_v is fixed for a given z_m . The value of z_m can be obtained by the assumption that the age of the universe at the turnaround of a halo (t_m) is half the age of the universe at its collapse (t_c): $t_m = t_c/2$. For a given redshift of halo collapse, z_c , the time t_c and the redshift z_m can be calculated from the redshift-time relation. This relation for an open universe is

$$t = H_0^{-1} \frac{(1 + \Omega_0 z)^{1/2}}{(1 - \Omega_0)(1 + z)} - \frac{\Omega_0}{2(1 - \Omega_0)^{3/2}} \ln \frac{(1 + \Omega_0 z)^{1/2} + (1 - \Omega_0)^{1/2}}{(1 + \Omega_0 z)^{1/2} - (1 - \Omega_0)^{1/2}}, \quad (B7)$$

and for a flat universe is

$$t = H_0^{-1} \frac{2}{3\lambda_0^{1/2}} \ln \left\{ \frac{[\lambda_0(1 + z)^{-3}]^{1/2} + [\lambda_0(1 + z)^{-3} + \Omega_0]^{1/2}}{\Omega_0^{1/2}} \right\}. \quad (B8)$$

Table 1. Simulation Parameters

Model	Realizations	Ω_0	λ_0	Γ	σ_8	$L[h^{-1}\text{Mpc}]$	N_p	$\epsilon[h^{-1}\text{Mpc}]$
SCDM0.62	3	1.0	0.0	0.5	0.62	128	100^3	0.1
B-SCDM0.62	5	1.0	0.0	0.5	0.62	300	128^3	0.2
SCDM1.24	5	1.0	0.0	0.5	1.24	300	128^3	0.2
FLAT	5	0.2	0.8	0.2	1.00	128	64^3	0.1
OPEN	5	0.2	0.0	0.2	1.00	128	64^3	0.1

Table 2. The Values of $\langle v_1^2 \rangle^{1/2}$, Q and γ

Model	$\langle v_1^2 \rangle^{1/2}$ (model)	$\langle v_1^2 \rangle^{1/2}$ (simulation)	Q	γ
SCDM0.62	713 [762]	714 ± 22	1.46	1.74
B-SCDM0.62	742 [762]	694 ± 12	1.46	1.74
SCDM1.24	1464 [1482]	1380 ± 33	1.55	1.72
FLAT	521 [595]	524 ± 21	1.78	1.75
OPEN	571 [642]	556 ± 28	1.42	1.77

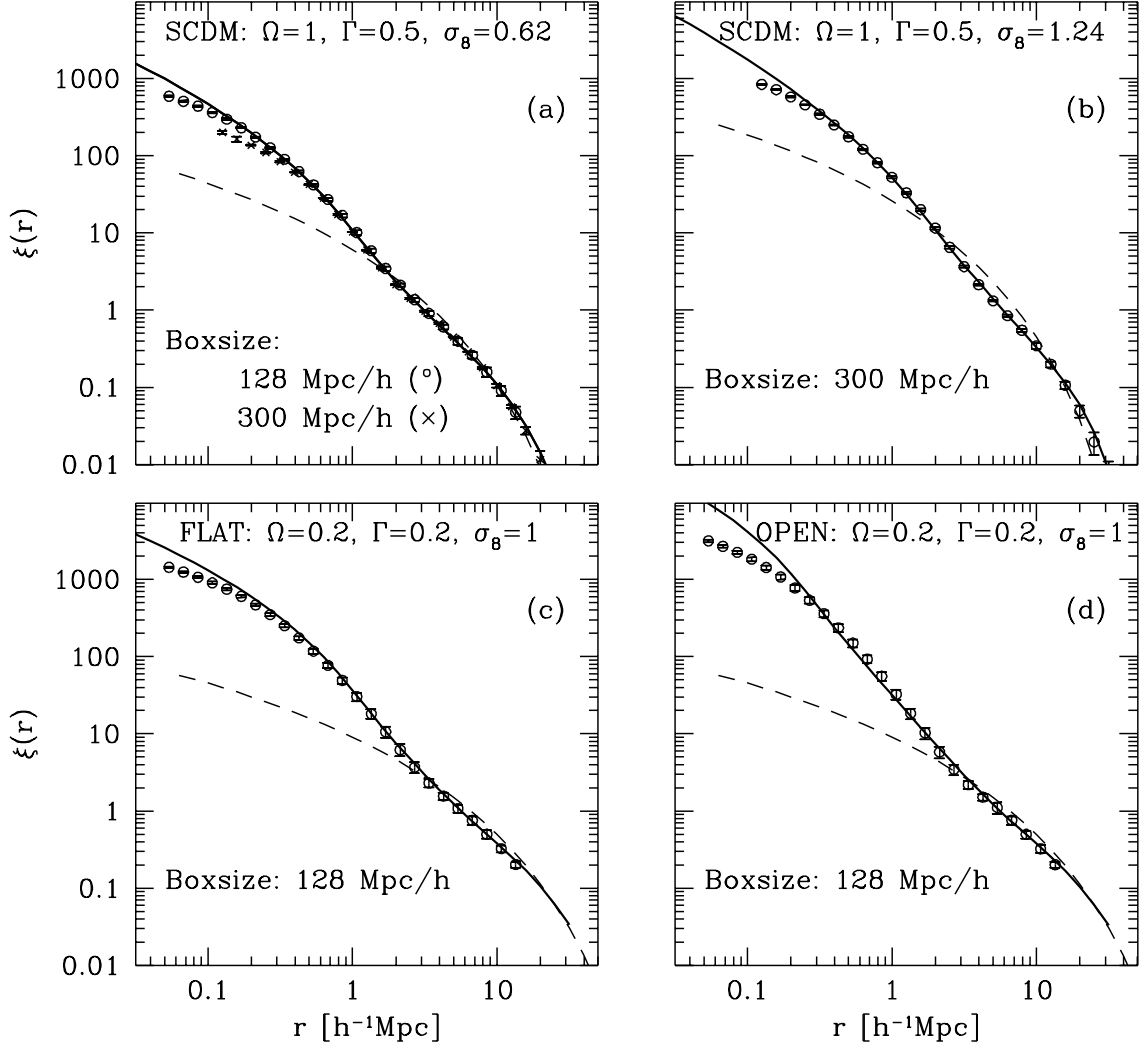


Fig. 1.— The two-point correlation functions of dark matter particles predicted by the analytical model (solid curves) compared to the results derived from N-body simulations (symbols). The dashed curves show the two-point correlation functions given by the linear power spectra. The error bars show the scatter among different realizations. The model parameters and the simulation box sizes are indicated in each panel.

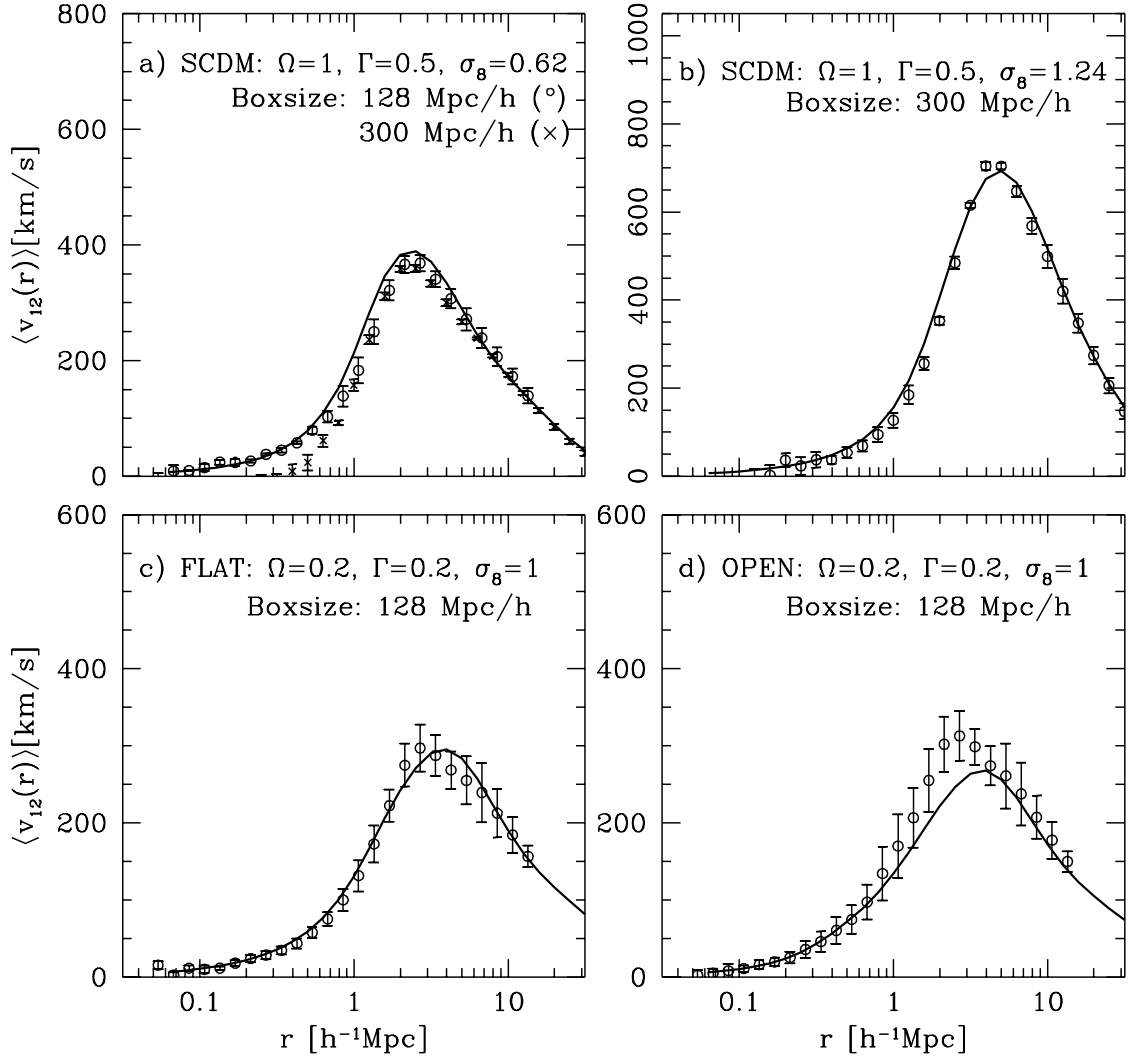


Fig. 2.— The average pairwise peculiar velocity of dark matter particles predicted by the analytical model (solid curves) compared to the results derived from N-body simulations (symbols). The error bars show the scatter among different realizations

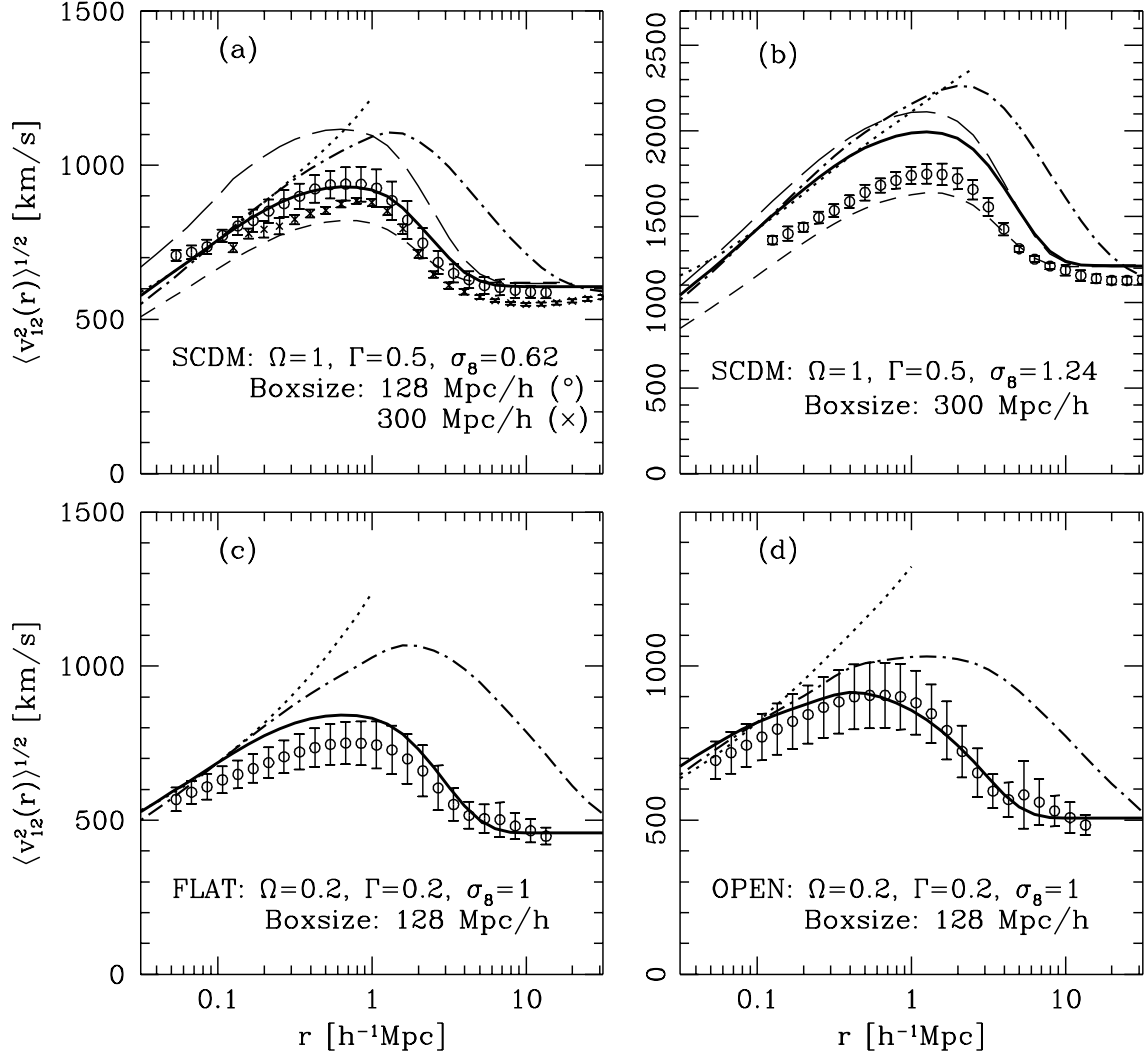


Fig. 3.— The pairwise peculiar velocity dispersion of dark matter particles predicted by the analytical model (curves) at the different stages of approximation (see Section 2.5.1). The dotted curves show the predictions of equation (23), while the dot-dashed and solid curves show the results given by equation (31) and equation (38), respectively. The two dashed curves (in a and b) show the predictions of equation (38) with the concentration factor $c = 5$ (lower curve) and 10. The symbols show results derived from N-body simulations. Error bars are the scatter among different realizations

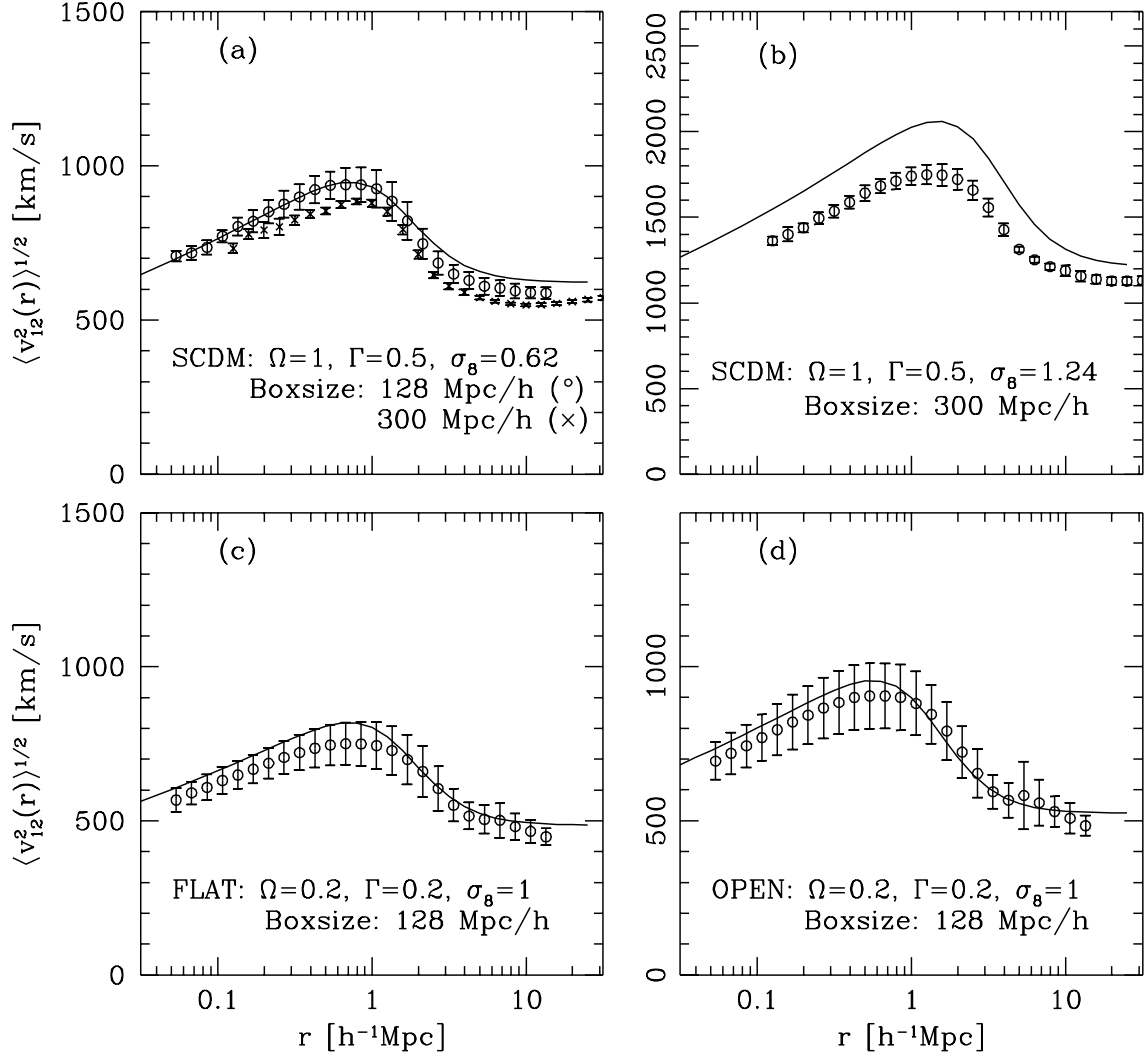


Fig. 4.— The pairwise peculiar velocity dispersion of dark matter particles given by the fitting formula (40) (curves), compared with the results derived from N-body simulations (symbols). Error bars are the scatter among different realizations

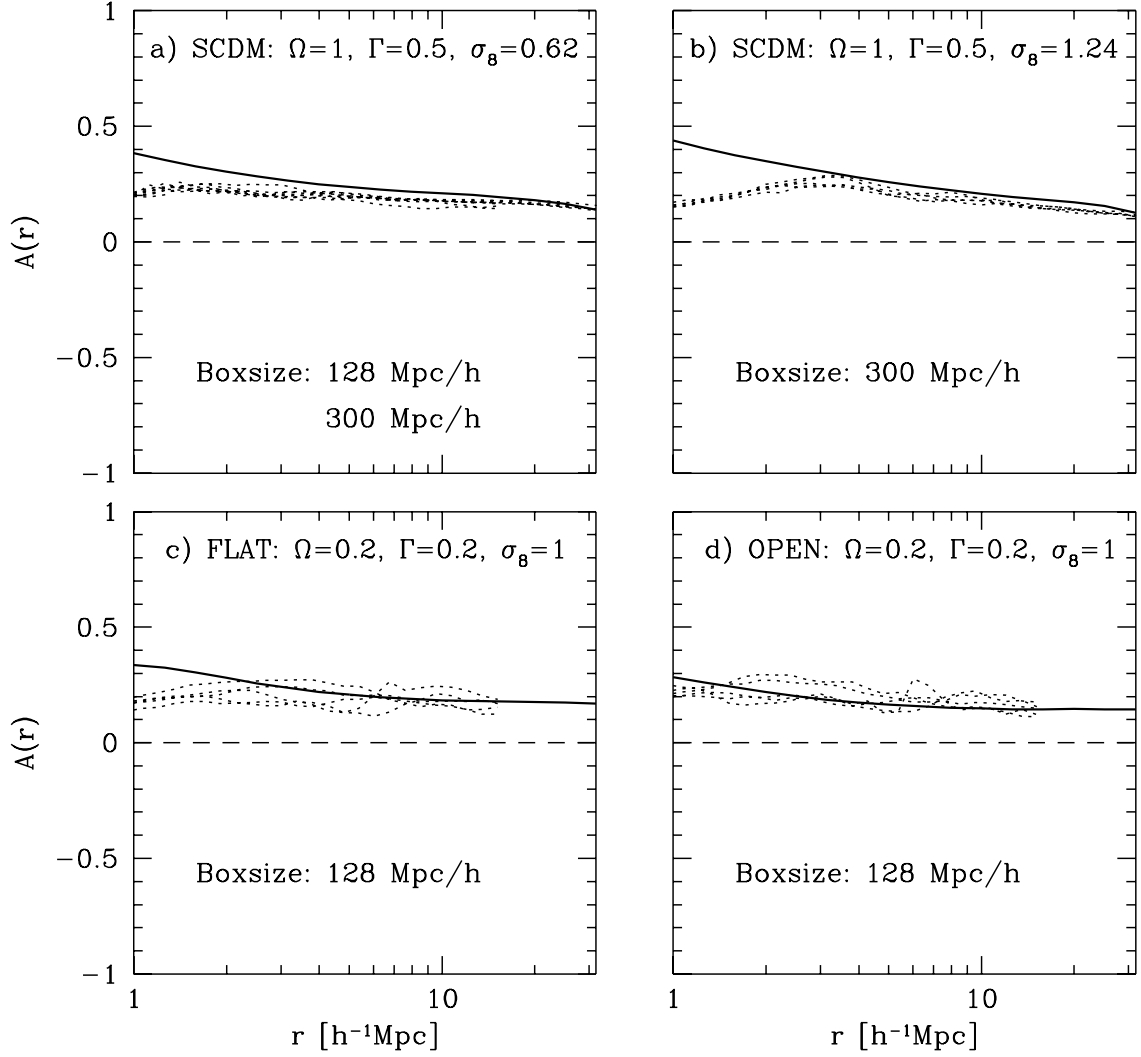


Fig. 5.— The velocity-dispersion anisotropy \mathcal{A} of dark matter particles predicted by the analytical model (solid curves) compared to the results derived from N-body simulations. Each dotted curve shows the result of simulation in one particular realization.

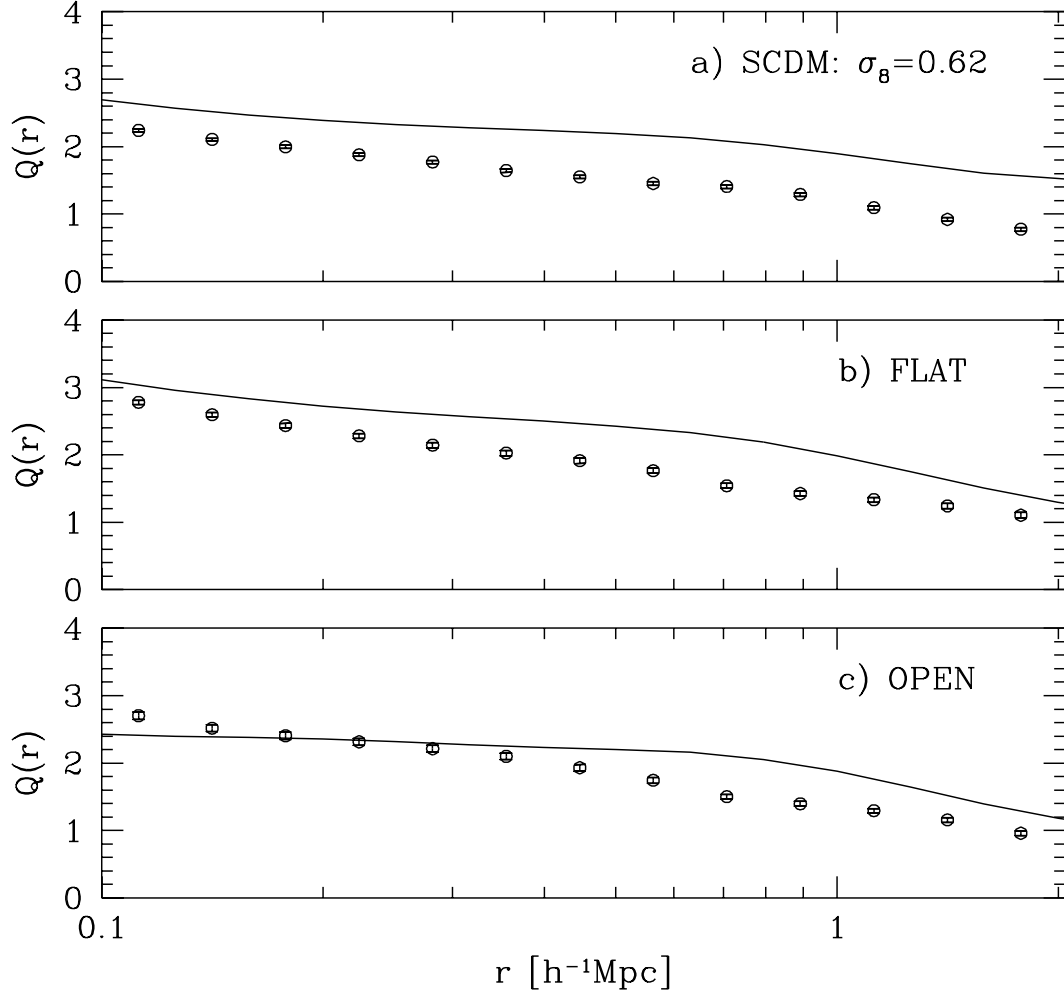


Fig. 6.— The amplitude of the three-point correlation function of dark matter particles predicted by the analytical model (solid curves) compared to the results derived from N-body simulations (symbols). The error bars are the scatter among different realizations

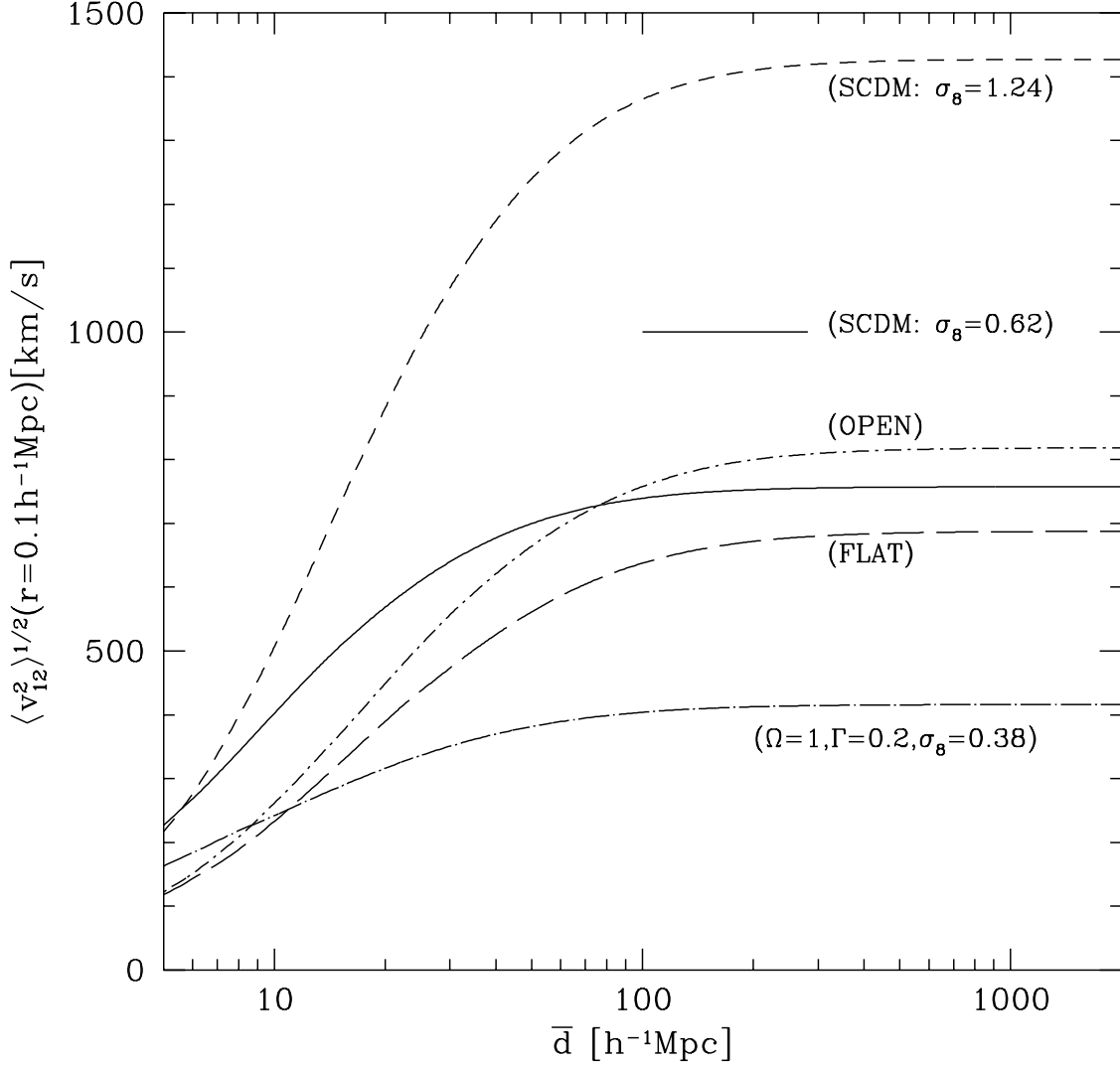


Fig. 7.— The pairwise peculiar velocity dispersion of dark matter particles at separation $r = 0.1 h^{-1}\text{Mpc}$ as a function of \bar{d} , the mean separation of haloes that are removed before the pairwise peculiar velocity dispersion is calculated. Results are shown for the SCDM models ($\Omega_0 = 1, \Gamma = 0.5$) with $\sigma_8 = 0.62$ and 1.24 , for FLAT and OPEN models ($\Omega_0 = 0.2, \Gamma = 0.2$) with $\sigma_8 = 1$ and for an additional model with $\Omega_0 = 1, \Gamma = 0.2$ and $\sigma_8 = 0.38$. The last three models have the same value of $\sigma_8 \Omega_0^{0.6}$.